FeS_2 (pyrite) electrodeposition thin films and study of growth mechanism

DONG Youzhong[1], ZHENG Yufeng[1], ZHANG Xiaogang[2], DUAN He[1], SUN Yanfei[1] & CHEN Yanhua[1]

1. Department of Physics, Xinjiang University, Urumqi 830046, China;
2. Institute of Applied Chemistry, Xinjiang University, Urumqi 830046, China
Correspondence should be addressed to Zheng Yufeng (email: zyf2616@163.com)

Received August 20, 2004

Abstract Ferrous sulfide (FeS) thin films were initially electrodeposited on indium-tin oxide (ITO) substrates in the aqueous solution containing iron, sulfur elements and then annealed in the sulfur atmosphere. Thereby, we successfully obtained the single-phased iron pyrite (FeS_2) thin films with good quality. The experimental parameters for electrodeposition and the post-growth thermal-dynamical conditions have been calculated so that more details about the effect of thermal-dynamical conditions on the micromechanism concerned with the iron pyrite crystal growth as well as the properties of the samples have been discussed.

Keywords: electrodeposition, FeS_2 (pyrite), thin films, growth dynamics.

DOI: 10.1360/102004-32

With the development of semiconductor solar cells, much attention has been focused on the low-cost, high-performance photovoltaic materials for solar cell fabrications. Sulfide compounds[1,2], due to their desirable optical properties, were widely used in preparing solar cells. Although the Cd-based II-VI compounds solar cell, such as CdS, CdTe, etc.[3,4], processes a higher conversion efficiency than the sulfide-based solar cell does. The iron pyrite (FeS_2) characteristic of suitable bandgap, $E_g = 0.95$ eV[5], very high absorption coefficient, $\alpha \geqslant 5\times105$ cm^{-1} for $\lambda \leqslant 700$ nm, as well as the abundant composite elements and stability, has been regarded as the most promising alternative solar cell material at the present. On the other hand, several methods have been applied for the preparation of the iron pyrite thin films: thermal evaporation[6,7], chemical spray pyrolysis[8], metal-organic chemical vapor deposition[9], sulfurization of Iron oxide films[10] and pure iron films[11−14], etc.

However, it has been suggested that in the preparation process FeS_2 can crystallize not only into a cubic pyrite structure, but also into an orthorhombic metastable marcasite structure that is detrimental to photovoltaic applications because of its low bandgap (E_g

= 0.3 eV[15]). Therefore, the preparation of high-quality, single-phased iron pyrite thin films is a most challenge for the research of the iron-pyrite-based solar cells. In this work, we successfully prepared singled-phased pyrite (FeS_2) thin films via annealing the electrodeposited ferrous sulfide (FeS) thin films in a sulfur atmosphere and obviated the reverse effect of the marcasite by-product. In addition, based on the structural characteristic and dynamics theory, we analyzed the micromechanism and the dependence of the growth rate on the sulfueradition thermal-dynamical conditions during the growth of iron pyrite. Compared with other methods, our experimental process is more controllable and convenient.

1 Experiments

The electrodeposition was carried out in the stirred solution potentiostatically and indium-tin oxide (ITO) substrate (area 2 cm^2, square resistance R =12.8 Ω/□, here □ is indium-tin oxide (ITO) substrate) was chosen as cathode, the platinum sheet as anode. The electrodeposition bath consists of aqueous solution containing $FeCl_2$ and $Na_2S_2O_3$. The concentration rate is $k = c(Fe^{2+}):c(S_2O_3^{-2})$, where $c(Fe^{2+})$ is the concentration of $FeCl_2$ solution, $c(S_2O_3^{-2})$ is the concentration of $Na_2S_2O_3$ solution. The pH value of the solution was adjusted by adding dilute hydrochloric acid or dilute sodium hydrate. The parameters which influence greatly the performance of pyrite thin films are the concentration rate k and the pH value of the solution and they are calculated by theory formula. Ferrous sulfide (FeS) thin films were prepared on such conditions. The annealing treatment in a sulfur atmosphere was performed in a closed quartz tube at different temperatures (sufur pressure 8.0 kPa) and varied annealing time from 30 to 60 min. In order to prevent peeling, we controlled the increasing temperature rate less than 4℃/min and decreasing temperature less than ≤2℃/min. The X-ray powder diffraction patterns were recorded on a Japan Mac Science 18 kW rotation anode X-ray diffractometer with Cukα1 radiation. The morphology of the samples was investigated by scanning electronic microscopy (SEM), with the images being taken with a German leo1430vp scanning electronic microscope. The electric properties were determined by a HL5500 Hall auto-measuring appliance in magnetic induction of 0.32 T.

2 Results and discussion

2.1 Preparation parameters and structural analysis of ferrous sulfide (FeS) thin films

(i) Theory analysis of preparation parameters of ferrous sulfide (FeS) thin films. Two reactions occur around the cathode during the electrodeposion of ferrous sulfide (FeS) thin films. One is deposition of the iron, and the other is deposition of the sulfur. The corresponding reaction equations are as follows:

$$Fe^{2+} + 2e = Fe, \qquad S_2O_3^{2-} + 6H^+ + 4e = 2S + 3H_2O.$$

According to the Nernst equation, equilibrium electrode potential E is fit into the fol-

lowing equation[16]:

$$E = E^0 + \frac{RT}{nF}\ln\frac{\alpha\ (\text{oxidation-state})}{\alpha\ (\text{deoxidize-state})},$$

where E^0 is the standard potential of the electrode system, $\frac{RT}{F} = 0.05917$, R the gas constant, T the experiment temperature, F the Faraday constant, n the electron amount of participation reaction, and $\frac{\alpha(\text{oxidation}-\text{state})}{\alpha(\text{deoxidize}-\text{state})}$ is the ratio of the product of all the oxidation state concentration or the disoxidation state concentration.

For iron: $n = 2$, the concentration of iron ion $\alpha(Fe^{2+}) = 0.225$ mol/L, $E^0 = -0.44$ V. At 25℃ the equilibrium electrode potential can be expressed as

$$\begin{aligned} E(Fe^{2+}/Fe) &= E^0 + (0.05917/2)\ln[\alpha(Fe^{2+})] \\ &= -0.44 + 0.02958\ln[\alpha(Fe^{2+})]. \end{aligned}$$

While for sulfur: $n = 4$, the concentration of the thiosulfuric acid radical ion $\alpha(S_2O_3^{2-}) = 0.45$ mol/L, $E^0 = 0.50$ V. At 25℃ equilibrium electrode potential can be written as

$$\begin{aligned} E(S_2O_3^{2-}/S) &= E^0 + (0.05917/4)\ln\{\alpha(S_2O_3^{2-})\times[\alpha(H^+)]^6\} \\ &= 0.50 + 0.01479\ln\{\alpha(S_2O_3^{2-})\times[\alpha(H^+)]^6\}. \end{aligned}$$

In addition, because of the influence of the polarization action there exists some differences between the deposition potential of both iron and sulfur and the equilibrium electrode potential, which results in overpontential (the overpotentail of the cathode equals to the equilibrium electrode potential minus the deposition potential). According to the experimental data, the calculated overpotentail value for iron and sulfur deposited on the ITO substrates is 0.2198 and 0.8194 eV respectively. In order to obtain FeS films, the codeposition conditions for iron and sulfur must be satisfied simultaneously. That is, their individual deposition potential is expected to be equal, where the deposition potential equals to the equilibrium potential minus the overpotential:

$$E(Fe^{2+}/Fe) - 0.2198 = E(S_2O_3^{2-}/S) - 0.8194.$$

Therefore,

$$\ln\{[\alpha(Fe^{2+})]^2/[\alpha(S_2O_3^{2-})]\} - 6\ln[\alpha(H^+)] = 23.0156.$$

Considering the above equations, we can infer that the concentration of H^+ or the pH value of the solution has more impact on the codeposition of iron and sulfur than the concentration of Fe^{2+} and $S_2O_3^{2-}$. Thus, when the pH value of the solution is about 1.824 and the concentration of $FeCl_2$ and $Na_2S_2O_3$ solution is 0.225 and 0.45 mol/L respectively (k = 1:2), the codeposition of iron and sulfur can be carried out to fruition.

(ii) XRD and SEM analysis of the ferrous sulfide (FeS) thin films. Fig. 1 is the X-ray diffraction profiles of the FeS thin films. Except some intensive peaks corresponding to ITO substrate, other peaks can be characterized as FeS whose intensity is rather weak. Fig. 2 is the SEM micrograph of the FeS samples. It can be seen that the resulted thin film is mainly composed of an aggregate of agglomerate grains with uneven grain sizes and irregular shapes, which are conglutinative to each other. Some small pins in the film can also be observed, which confirms the incompactness of the electrodeposited FeS thin film.

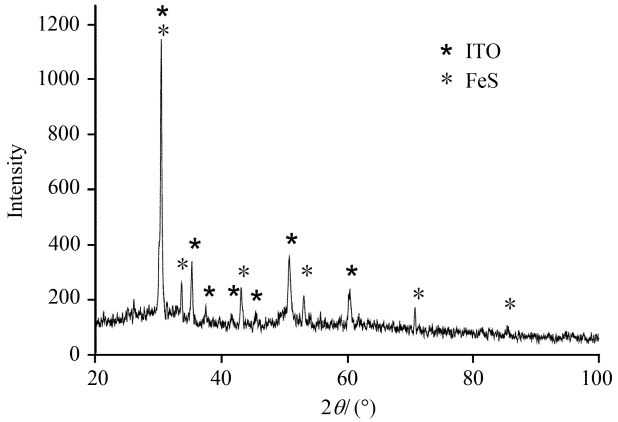

Fig. 1. XRD profiles of the FeS thin films.

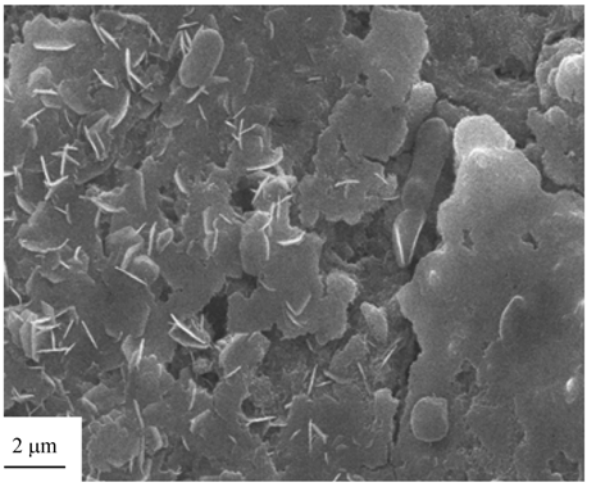

Fig. 2. SEM micrograph of the FeS thin films.

2.2 Structural and property change of the sample in sulfuring progress

(i) Structural change of the sample in sulfuring progress. Fig. 3 shows the XRD patterns of the resulted thin films annealed in a sulfur atmosphere at 200℃, 300℃, 400℃, 500℃ and 600℃ respectively. For comparison, the XRD pattern derived from

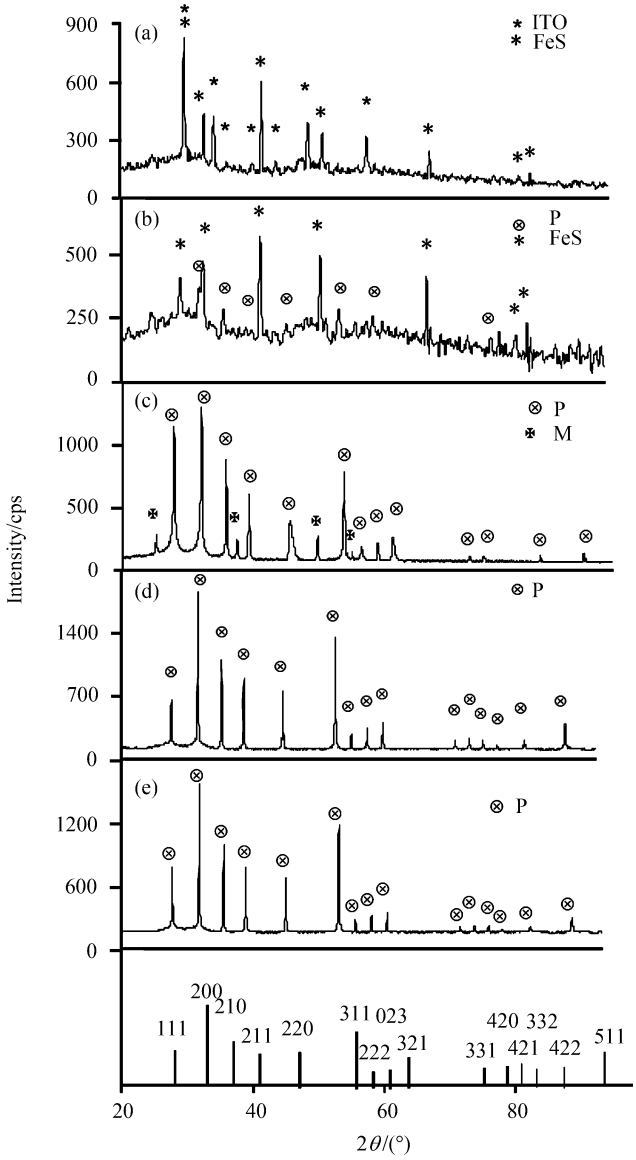

Fig. 3. XRD patterns of the sample sulfidated under different temperatures (P: Pyrite, M: Marcasite).

the standard ASTM71-2219 card is also given in this figure. Annealing at 200℃ cannot supply sulfur and ferrous sulfide with sufficient energy to form the iron pyrite phase, which leads to the absorption of the majority of sulfur atoms on the surface of ferrous sulfide thin films. As a result, the peaks of the pyrite are almost unobservable. The thin film annealed at 300℃ tends to be compact on the grounds that the peaks of ITO substrates entirely disappear. At the same time, the sulfuration reaction occurs and the peaks of the pyrite corresponding to (200), (210), (211), (220), and (311) crystal planes can be clearly observed in spite of their weak intensities as the result of the imperfection of the

on-going pyrite crystallization. When the FeS thin films were annealed at 400℃, the insufficient sulfuration process leads to the formation of the transitional phase marcasite. With the annealing temperature rising from 500℃ to 600℃, it is found from Fig. 3 that the films annealed at 500℃ consists of singled-phased pyrite without any contributions from marcasite, which indicates that the conversion from the marcasite phase to the pyrite phase as the rising annealing temperature. At a higher temperature (600℃), there is no apparent change in the intensity of the pyrite peaks. According to the above discussion, we can conclude that 500℃ is the most suitable annealing temperature for the formation of the single-phased pyrite.

Fig. 4(a) shows the asymmetry factor *A* of diffraction peaks, which is defined as *b/a*. The asymmetry of (200), (210), (211), (220), and (311) of diffraction peaks correspond-

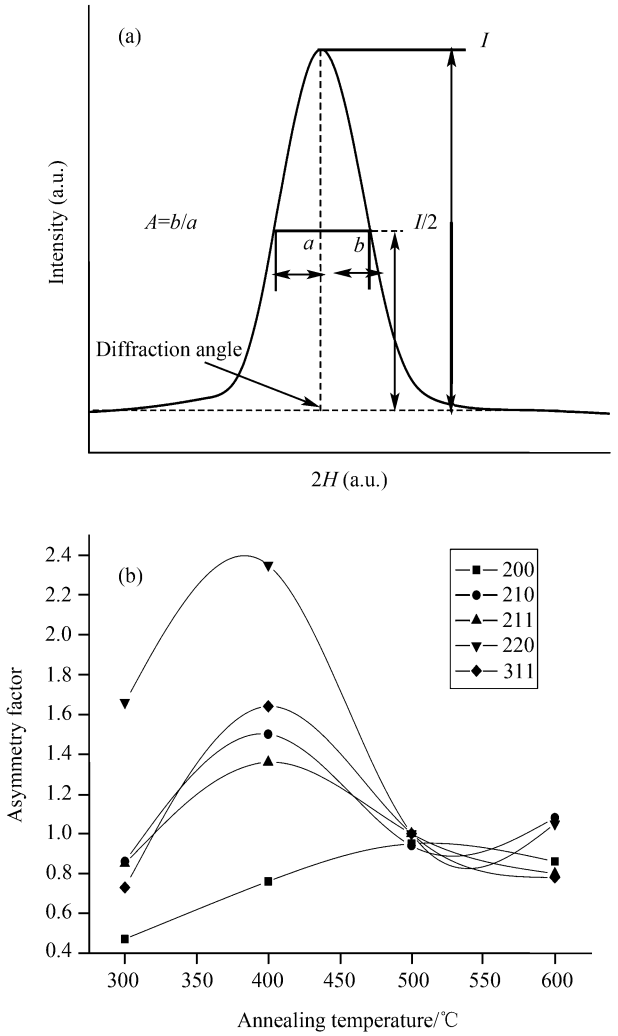

Fig. 4. (a) Denotation of asymmetry factor for diffraction peaks. (b) The transformation case of the asymmetry factor at different annealing temperature.

ing to pyrite films annealed at different temperature is depicted in Fig. 4(b). It is noticed that the annealing temperature exerts significant influence on the value of A. But at 500℃, the values of A almost approximate to 1 and each corresponding peak exhibits perfect symmetry. So it is confirmed that the fully-fledged pyrite grains lead to lesser interior defeats and lattice distortion in the pyrite crystals.

(ii) Dynamics analysis in sulfuring process. Fig. 5 shows the dependence of the pyrite grain size on the annealing time. The value of grain sizes is deduced from Scherrer's formular[17]. From this figure, we can see that the curve of $D_A - t$ represented different annealing temperatures is of ascending tendency, which implies that the sulfuring process offers favorable dynamical conditions for pyrite growth. It is noted that the growth rate increases dramatically at the initial stage, and then decreases gradually as the annealing time is extended.

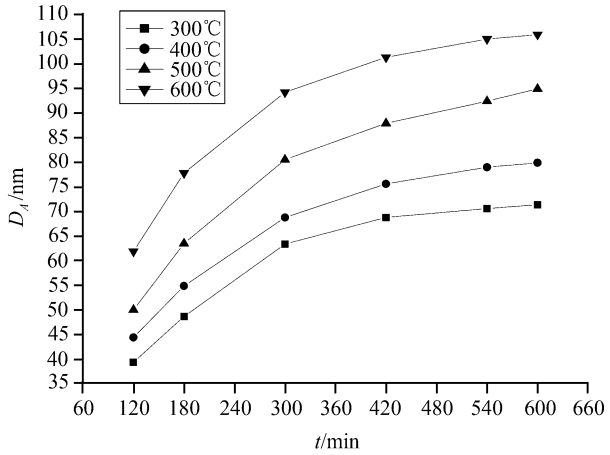

Fig. 5. The relation between grain sizes of pyrite and reactor time at different sulfuring temperature.

The growth dynamic law is generally applied to explain the relating growth mechanism, and the growth rate can be written out as follows[18]:

$$D_A^{\,2} - D_{A0}^{\,2} = K_T \cdot t^{\varphi}, \tag{1}$$

where D_{A0} is the initial pyrite grain size, K_T is the growth rate constants, and φ is time index. According to Johuson-Mehl-Avrami equation[19], K_T can be expressed as

$$K_T = K_0 \exp(-E_A/RT), \tag{2}$$

where K_0 is a constant, E_A is apparent growth activity energy of ions in the crystal, R is the gas constants, and T is the temperature. Within the limits of experiments, $D_{A0}^{\,2} << D_A^{\,2}$, we can derive eq. (3) by combining eq. (1) and eq. (2):

$$2\ln D_A = \ln K_0 + \varphi \ln t - E_A/RT. \tag{3}$$

Fig. 6 shows the linearity relationship between $2\ln D_A$ and $1/T$, which indicates that the law of grain growth is accordant with the quadratic equation. We derive the apparent

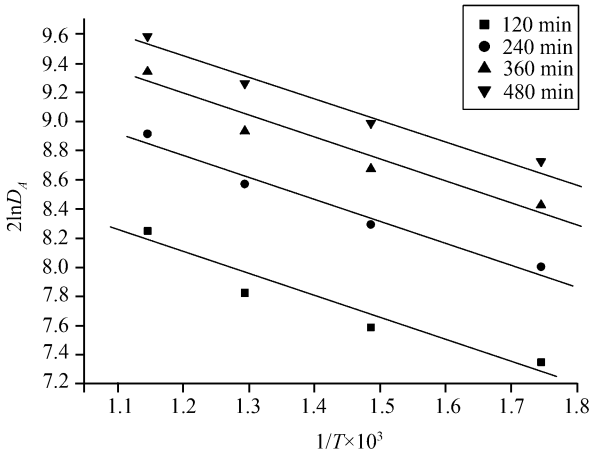

Fig. 6. The relation of 2lnD_A and 1/T

growth activity energy of the grains from the slop of each straight line and the results are listed in Table 1. We can see that sulfuring time has a negligible effects on E_A and the calculated average value of E_A is 11.96 kJ/mol.

Table 1 Thermal dynamic parameters of growth for pyrite grain

T/K	E_A/kJ · mol	φ	K_T/nm^2 · $t^{-1.022}$
573	11.56	1.010	12.15
673	11.94	1.025	14.37
773	12.19	1.033	17.61
873	12.14	1.018	25.70

Fig. 7 shows the relationship between 2lnD_A and ln$t$, and we can approximately calculate the average time index ($\varphi = 1.022$). Thus we can deduce that the square of the pyrite grain size is proportional to $t^{1.022}$ and the corresponding crystal growth is a decelerated increasing process.

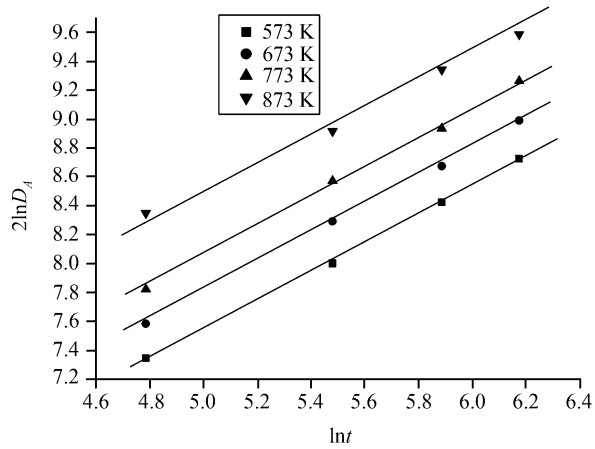

Fig. 7. The relation of 2lnD_A and ln$t$.

This can be interpreted from the nucleation and growth mechanism. Because the nucleation formation of pyrite occurs on the surface of FeS grains while the growth process is related to the extension into the FeS grains. So the growth of pyrite can be regarded as a process of the merging of the FeS grains, in which the mechanism in relation to the diffusion of the formed pyrite grains is rather complicated. On the other hand, because the longer annealing time contributes the decrease not only in the number of the FeS grains, but in the probability of the contact and merging between pyrite grains, which promotes the pyrite crystal perfection, the final growth rate is to be decreased gradually.

In order to obtain the growth rate of the pyrite grains, we determine the value of K_T at different annealing temperatures via the intercept of the line in Fig. 7. The results are listed in Table 1.

(iii) The change of electric property of sample during sulfuring process. Fig. 8 is the relationship of the annealing time and the resistance of the samples annealed at 500℃. We can see from this figure that the resistance decreases significantly when the annealing time rises from 60 to 180 min (AB stage), and then it just keeps invariable until the annealing time is up to 300 min when the resistance of sample increases appreciably. This phenomenon can be explained based on the mechanism of the pyrite crystallization.

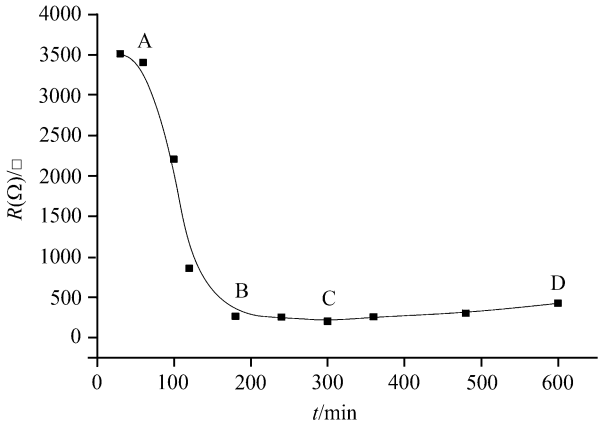

Fig. 8. The relation of the square resistance and annealing time of the sample.

The nucleation, growth and roughness of the pyrite grain can account for a process accompanied by the nucleation and the transformation of crystal phases, interfaces and the grain boundaries. This process will generally influence the properties of the electric transport especially of the resistance of the crystal system[20].

At the nucleation stage, the pyrite nucleus are formed by reacting between FeS grains and sulfur atoms which diffuses into the grain boundary of FeS, so that FeS grains are packed by the surrounding of the pyrite crystal nucleus. The larger the grain boundary regions result in the considerable high square resistance, the longer the annealing time makes it easier for sulfur atoms to diffuse into the interior to react with the FeS grains. Thus, the grain sizes of the pyrite become enlarged with the reduction of the grain

boundary region, which leads to a lower resistance of the sample (AB part in Fig. 8). Moreover, the different configurations of sulfur atoms in both FeS and FeS_2 grains result in an obvious change of the resistance of samples during the phase of the pyrite nucleus formation and the crystal growth. At the primary stage, FeS is the main phase and the rather higher square resistance of samples can be achieved, while during the latter stage, the conversion from FeS to pyrite makes the sample square resistances decrease abruptly. The flat region in the middle part of the curve (BC part in Fig. 8) implies that the indistinctive change of the grain boundaries in spite of the remarkable increase of the pyrite grain sizes has occurred. However, the merging of the pyrite grains with each other might well lead to the formation of new grain boundaries (pyrite grain boundary). As a result, the resistance of the sample increases slightly (CD part in Fig. 8).

3 Conclusion

In this paper, we presented a readily available method for the preparation of the single-phased iron pyrite with good uniformity and compaction thin films via annealing the electrodeposited ferrous sulfide thin films in a sulfur atmosphere. Several conclusions can be drawn from the above analysis: when concentration rate k is 1:2, the pH value of the solution is about 1.824 in order to carry out the codeposition of iron and sulfur. The sulfuring temperature is supposed to be crucial to the conversion from FeS to FeS_2, and the optimal annealing temperature is determined at 500℃. The growth dynamics of the pyrite grains is proved to accord with the quadratic equation. The apparent activation energy of the grain is about 11.96 kJ/mol and time factor (φ) is 1.022.

Acknowledgements This work was supported by the National Natural Science Foundation of China (Grant No. 50062002).

References

1. Fang, X. S., Ye, C. H., Zhang, L. D. et al., Temperature-controlled catalytic growth of ZnS nanostructures by the evaporation of ZnS nanopowders, Adv. Funct. Mater, 2005, 15(1): 63－68.[DOI]
2. Chen Yanhua, Zheng Yufeng, Zhang Xianggang et al., Solvothermal synthesis of nanocrystalline FeS_2, Science in China, Ser. G, 2005, 48(2): 188－200. [Abstract]
3. Savadogo, O., Chemically and electrochemically deposited thin films for solar energy materials, Solar Energy Materials and Solar Cells, 1998, 52: 361－388. [DOI]
4. Li Bing, Feng Liangheng, Zheng Jiagui et al., The preparation and property of CdS thin films, Chinese Journal of Semiconductors, 2003, 24(8): 837－840.
5. Ennaoui, A., Fiechter, S., Pettenkofer, C. et al., Iron disulfide for solar energy conversion, Solar Energy Materials&Solar Cells, 1993, (29): 289－295.
6. Delas Heras, C., S'anchez, C., Characterization of iron pyrite thin films obtained by flash evaporation, Thin Solid Films, 1991, 199(2): 259－267. [DOI]
7. Delas Heras, C., Ferrer, I. J., S'anchez, C., Pyrite thin films: Improvements in their optical and electrical properties by annealing at different temperatures in a sulfur atmosphere, J. Appl. Phys., 1993, 74(7): 4551－4556. [DOI]
8. Smestad, G.,Da Silva, A., Tribusch, H. et al., Formation of semiconducting iron pyrite by spray pyrolysis, Solar Energy Materials, 1989, 18(5): 299－313. [DOI]
9. Chatzitheodorou, G., Fiechter, S., Kunst, M. et al., Low temperature chemical preparation of semiconducting

transition metal chalcogenide films for energy conversion and storage, lubrication and surface protection, M at Res. Bull., 1988, 23(9): 1261－1271. [DOI]

10. Smestad, G., Ennaoui, A., Fiechter, S. et al., Photoactive thin film semiconducting iron pyrite prepared by sulfurization of iron oxides, Solar Energy Materials, 1990, 20(3): 149－165. [DOI]
11. Bausch, S., Sailer, B., Keppner, H. et al., Preparation of pyrite films by plasma-assisted sulfurization of thin iron films, Appl. Phys. Lett., 1990, 57(1): 25－27. [DOI]
12. Ferrer, I. J., S'anchez, C., Characterization of FeS_2 thin films prepared by thermal sulfuration of flash evaporated iron, J. Appl. Phys., 1991, 70(5): 2641－2647. [DOI]
13. Delas Heras, Mart in de Vidales, J. L., Ferrer, I. J. et al., Structural and microstructural features of pyrite FeS_2-X thin films obtained by thermal sulfuration of iron, J. Mater. Res., 1996, 11(1): 21－220.
14. Liu, Y. H., Meng, L., Zhang, L. et al., Optical and electrical properties of FeS2 thin films with different thickness prepared by sulfurizing evaporated iron, Thin Solid Film, 2005, 479(1-2): 83－88. [DOI]
15. Sigeyuki, N., Akio, Y., Electrodeposition of pyrite(FeS_2) thin films for photovoltaic cells, Solar Energy Materials & Solar Cells, 2001, 65: 79－85. [DOI]
16. Fu Xiancai, Sheng Wenxia, Yao Tianyang, Physical chemistry (Fourth Edition), Undervolum, Beijing: Higher Education Press, 1999, 601.
17. Fan Xun, Metal X-ray Study, Beijing: Mechanical Industry Press, 1989, 103.
18. Liu Hezhou, Hu Wenbing, Gu Mingyuan et al., The growth dynamics study of TiO_2 nano grains, Journal of Inorganic Materials, 2002, 17(3): 429－436.
19. Avrami, Mehl, Kinetics of Phase Change. II Transformation-Time Relations for Random Distribution of Nuclei, J. Chem. Phys., 1940, 8(2): 212－224.
20. Wang Yaping, Lu Ke, The study of high precision resistance inspection in nucleation process of amorphous material alloy, Science in China, Ser. E, 2000, 30(3): 193－199.